Chaos-induced enhancement of resonant multielectron recombination in highly charged ions: Statistical theory

V. A. Dzuba,[1] V. V. Flambaum,[1] G. F. Gribakin,[2] and C. Harabati[1]

[1]*School of Physics, University of New South Wales, Sydney 2052, Australia*
[2]*Department of Applied Mathematics and Theoretical Physics, Queen's University, Belfast BT7 1NN, Northern Ireland, United Kingdom*

A statistical theory of resonant multielectron recombination based on properties of chaotic eigenstates is developed. The level density of many-body states increases exponentially with the number of excited electrons. When the residual electron-electron interaction exceeds the interval between these levels, the eigenstates (called compound states or compound resonances if these states are in the continuum) become "chaotic" superpositions of large numbers of Hartree-Fock configurational basis states. This situation takes place in some rare-earth atoms and many open-shell multiply charged ions excited in the process of electron recombination. Our theory describes resonant multielectron recombination via dielectronic doorway states leading to such compound resonances. The result is a radiative capture cross section averaged over a small energy interval containing several compound resonances. In many cases individual resonances are not resolved experimentally (since the interval between them is small, e.g., $\leqslant 1$ meV, possibly even smaller than their radiative widths); therefore, our statistical theory should correctly describe the experimental data. We perform numerical calculations of the recombination cross sections for tungsten ions W^{q+}, $q = 18$–25. The recombination rate for W^{20+} measured recently [Schippers *et al*. Phys. Rev. A **83**, 012711 (2011)] is 10^3 greater than the direct radiative recombination rate at low energies, and our result for W^{20+} agrees with the measurements.

PACS number(s): 34.80.Lx, 31.10.+z, 34.10.+x, 32.80.Zb

I. INTRODUCTION

The majority of atoms in highly excited states and many open-shell (e.g., rare-earth) atoms, even in vicinity of the ground state, behave as complex, chaotic many-electron systems. They are characterized by dense level spectra and strong configuration mixing. The corresponding many-electron wave functions are mixtures of large numbers of many-excited-electron basis states (Slater determinants) with nearly random mixing coefficients. Obtaining detailed information about such systems by standard theoretical methods, such as configuration interaction, becomes problematic because of the sheer size of the effective Hilbert space. In fact, the experiment often does not resolve individual energy levels, so a complete description is to some extent pointless.

On the other hand, such complex systems can be described using statistical approaches. Statistical methods for chaotic compound states are widely used in nuclear physics (see, e.g., Refs. [1–5]). Similar methods have been developed for open-shell atomic systems [6–9]. In particular, extensive numerical calculations were performed for the cerium atom to test the assumptions and predictions of the statistical theory [6]. These works examined the properties of the Hamiltonian matrix in chaotic many-body systems, statistics of energy-level spacings, dependence of mean orbital occupation numbers on the excitation energy, statistics and mean-squared values of electromagnetic amplitudes between chaotic many-body states, enhancement of weak perturbations in such states, and electronic and electromagnetic widths of chaotic compound resonances. Some aspects of the statistical theory were also tested for multicharged ions [7–9].

In the present paper we want to use the statistical theory to describe the effect of compound resonances on electron recombination with open-shell multicharged ions. Electron recombination is an important process in laboratory and cosmic plasmas, as well as in ion storage rings. Theory and experiment agree very well for relatively simple systems with one or two valence electrons above closed shells (see, e.g., Ref. [10]). For more complex systems theory and experiment often deviate significantly. For example, strong enhancements of the recombination rate were observed for Au^{25+} [11], U^{28+} [12], and W^{20+} [13] at low electron energies. For such ions the observed recombination rate is orders of magnitude greater than that due to direct radiative recombination (RR). In simpler systems the enhancement is due to resonant dielectronic recombination, though even for ions like $Fe^{9+} 3p^5$ and $Fe^{10+} 3p^4$, the dielectronic recombination appears to be deficient [14]. In complex open-shell ions such as $Au^{25+} 4f^8$ and isoelectronic W^{20+}, the absolute majority of the resonances correspond to many-excited-electron eigenstates which have very high density (exponentially small level spacings). In Refs. [7,8] we used a statistical approach to show that a factor of 200 enhancement over RR observed in Au^{25+} [11] is due to electron capture in these compound resonances.

In this paper we use the statistical theory to calculate the recombination rates for tungsten ions W^{q+}, $q = 18$–25. Our results for W^{20+}, where the measured rate at low (~ 1 eV) energies is 10^3 times higher than the radiative rate [13], are in good agreement with experiment. For other tungsten ions we predict similarly strong enhancements of the recombination rate.

A detailed derivation of the statistical theory for the recombination cross section is presented in the next section. Numerical calculations based on our statistical theory are somewhat similar to those of standard dielectronic recombination. However, in the statistical theory one does not need to diagonalize potentially very large Hamiltonian matrices for the excited states of the compound ion. Instead, the statistical
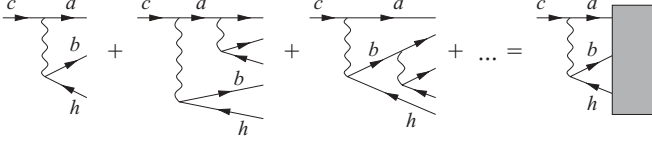
FIG. 1. Schematic diagram of electron capture into a strongly mixed multiconfigurational eigenstate (shaded block) through a dielectronic doorway configuration $h^{-1}ab$. Wavy lines show the Coulomb interactions.

formalism contains new parameters, namely, the *spreading width* Γ_{spr} and average electron orbital occupation numbers in the initial (ground) state of the ion. The total cross section of electron capture into compound resonances is given by

$$\bar{\sigma}_c = \frac{\pi^2}{2k^2} \sum_{abh,lj} \Gamma_{\text{spr}} \frac{|\langle a,b|\hat{v}|h,\varepsilon lj\rangle - \langle b,a|\hat{v}|h,\varepsilon lj\rangle|^2}{(\varepsilon - \varepsilon_a - \varepsilon_b + \varepsilon_h)^2 + \Gamma_{\text{spr}}^2/4}$$
$$\times \langle \hat{n}_h \hat{n}_c (1 - \hat{n}_a)(1 - \hat{n}_b)\rangle_i, \tag{1}$$

where ε and k are the energy and wave number of the incident electron; $\langle a,b|\hat{v}|h,\varepsilon lj\rangle$ and $\langle b,a|\hat{v}|h,\varepsilon lj\rangle$ are the direct and exchange Coulomb matrix elements, respectively; the sum is over the single-particle states (orbitals) of the hole (h) and excited electrons (a and b), and the partial waves lj of the incident, continuous spectrum electron (c); and $\hat{n}_a$, $\hat{n}_b$, etc., are the corresponding occupation numbers. The expectation value $\langle \hat{n}_h \hat{n}_c (1 - \hat{n}_a)(1 - \hat{n}_b)\rangle_i$ over the initial target state tells one that to transfer electrons from orbitals h and c into a and b, the former must be at least partially occupied and the latter at least partially empty. The continuum electron wave function c is normalized to the δ function of energy and $\hat{n}_c = 1$.

The presence of the spreading width in Eq. (1) is due to the fact that the two-electron–one-hole excitation $h^{-1}ab$ is not an eigenstate of the highly excited ion. This state is embedded in the dense spectrum of other, multiply excited states and is strongly mixed with them. This dielectronic state plays the role of a *doorway* state which "decays" to more complicated states, and the width of this "internal" decay is denoted by Γ_{spr}. This process is faster than either autoionization or radiative decay ("external" decays), and Γ_{spr} is greater than the autoionization or radiative widths (see below).

Figure 1 presents a perturbative, diagrammatic picture of electron capture through the doorway $h^{-1}ab$. In this temporal picture the process looks as a series of electron collisions. The initial electron c collides with an atomic electron in state h and excites it into state b. Then one of the excited electrons interacts with another atomic electron to produce more excitations, etc. As a result, the initial electron energy is shared between many electrons, and none of them has enough energy to escape. In this way a long-lived compound resonance is formed. A similar picture of neutron capture by nuclei dates back to Niels Bohr [15] and is very well known to nuclear physicists. This temporal picture assumes that individual time steps δt can be resolved. However, the uncertainty relation, $\delta t \delta E \gtrsim \hbar$, would then require a large energy uncertainty δE. In the recombination process the total energy of the system "electron + ion" is well defined. This means that all the components (steps in the process in Fig. 1) are present in the long-lived quasistationary compound state which captures

the electron. The language of strong configuration mixing is more appropriate in this case. With a perfect energy resolution one would see a very dense spectrum of narrow, possibly overlapping resonances. Broad doorway dielectronic states (with width Γ_{spr}) can only introduce a variation of the average height of these narrow compound resonances on the energy scale $\Delta\varepsilon \sim \Gamma_{\text{spr}}$.

Compared with the total resonant capture cross section, the recombination cross section

$$\bar{\sigma}_r = \omega_f \bar{\sigma}_c \tag{2}$$

contains an additional factor ω_f, known as the fluorescence yield. It accounts for the probability of radiative stabilization of the resonances (as opposed to autoionization) and is given by

$$\omega_f = \frac{\Gamma^{(r)}}{\Gamma^{(r)} + \Gamma^{(a)}}, \tag{3}$$

where $\Gamma^{(r)}$ and $\Gamma^{(a)}$ are the resonance radiative and autoionization widths, respectively. Expressions for these quantities and for the spreading width are presented in the next section.

Note that the capture cross section (1) is not very sensitive to the specific value of the spreading width Γ_{spr}, which for multicharged ions is about 0.5 atomic units (a.u.) [7] (see Table I in Sec. III). After angular reduction of the Coulomb matrix elements in Eq. (1) [Sec. II, Eq. (30)], numerical calculations of the capture cross section are straightforward.

An additional simplification occurs in heavy open-shell ions like Au^{25+} and W^{20+}, which have almost unit fluorescence yield. Indeed, the compound states in these ions contain very large numbers of principal basis-state components, $N \sim 10^4$. Each component contributes to the radiative decay into a large number of states below this compound state. In contrast, only one or few dielectronic (doorway) state components have nonzero Coulomb matrix elements that allow electron autoionization into the continuum [see Fig. 1 and Eq. (1)]. Therefore, the autoionization width of the compound resonance is suppressed by the small weight factor $1/N$ of the dielectronic components in the compound state. This means that the captured low-energy electron cannot escape, i.e., after the capture the radiative process happens with nearly 100% probability. (A similar effect in neutron capture by nuclei is described, e.g., in Ref. [16].) In this situation $\Gamma^{(a)} \ll \Gamma^{(r)}$ and $\omega_f \approx 1$, so that the electron recombination cross section, Eq. (2), is independent of the radiative width. In this regime one observes maximum chaos-induced enhancement of the resonant multielectron recombination. For example, the electron capture cross section calculated using Eq. (1) for Au^{25+} [8], was found to be in good agreement with experiment at low energies. On the other hand, in ions with a smaller number of active electrons, the number of components N may not be so large, leading to $\Gamma^{(a)} > \Gamma^{(r)}$ and $\omega_f < 1$.

II. THEORY

A. Resonant recombination cross section

The resonant radiative electron-ion recombination cross section is given by the sum over the resonances ν with the

angular momentum and parity J^π,

$$\sigma_r = \sum_\nu g(J)\sigma_\nu, \tag{4}$$

where $g(J) = (2J + 1)/[2(2J_i + 1)]$ is the probability factor due to random orientation of the electron spin and angular momentum J_i of the target ion [17]. The individual resonant contributions σ_ν are given by the Breit-Wigner formula [17],

$$\sigma_\nu = \frac{\pi}{k^2} \frac{\Gamma_\nu^{(a)} \Gamma_\nu^{(r)}}{(\varepsilon - \varepsilon_\nu)^2 + \Gamma_\nu^2/4}, \tag{5}$$

where $\Gamma_\nu^{(r)}$ is the the radiative decay rate (the total "inelastic width"), $\Gamma_\nu^{(a)}$ is the autoionization decay rate (the "elastic width"), and $\Gamma_\nu = \Gamma_\nu^{(r)} + \Gamma_\nu^{(a)}$ is the total width of the level ν. (We assume here that other inelastic channels, e.g., electronic excitation, are closed, which is correct at low incident electron energies.) The energy of the νth resonance is given relative to the ionization threshold I of the final compound ion, $\varepsilon_\nu = E_\nu - I$.

For systems with dense compound resonance spectra, the recombination cross section displays rapid energy dependence that may not even be resolved experimentally. Thus it is natural to average the cross section over an energy interval $\Delta\varepsilon$, which is large compared with the small mean level spacing D_{J^π} and the total resonance width, but much smaller than ε. This gives

$$\frac{1}{\Delta\varepsilon} \int \sigma_\nu d\varepsilon = \frac{2\pi^2}{k^2} \frac{\Gamma_\nu^{(r)} \Gamma_\nu^{(a)}}{\Delta\varepsilon \Gamma_\nu}, \tag{6}$$

where the integration limits are formally infinite, since the contribution of each resonance to the cross section decreases rapidly away from $\varepsilon \approx \varepsilon_\nu$. The number of resonances with a given J^π within $\Delta\varepsilon$ is $\Delta\varepsilon/D_{J^\pi}$, and after averaging, the recombination cross section (4) becomes

$$\bar{\sigma}_r = \frac{\pi^2}{k^2} \sum_{J^\pi} \frac{2J + 1}{(2J_i + 1)D_{J^\pi}} \left\langle \frac{\Gamma^{(r)}\Gamma^{(a)}}{\Gamma} \right\rangle. \tag{7}$$

Here $\langle \ldots \rangle$ means averaging of the width factor at the given energy.

If the fluorescence yield $\omega_f = \Gamma^{(r)}/\Gamma$ fluctuates weakly from resonance to resonance, the recombination cross section $\bar{\sigma}_r$ can be factorized, i.e., $\bar{\sigma}_c^r = \omega_f \bar{\sigma}_c$. For $\omega_f \approx 1$ the energy-averaged capture cross section

$$\bar{\sigma}_c = \frac{\pi^2}{k^2} \sum_{J^\pi} \frac{(2J + 1)}{(2J_i + 1)} \frac{\langle \Gamma^{(a)} \rangle}{D_{J^\pi}} \tag{8}$$

is the same as the recombination cross section.

In the opposite case of small radiative widths, autoionization dominates ($\Gamma^{(r)} \ll \Gamma^{(a)}$) and $\omega_f \ll 1$, so Eq. (7) yields the recombination cross section in the form

$$\bar{\sigma}_r^a = \frac{\pi^2}{k^2} \frac{\langle \Gamma^{(r)} \rangle}{(2J_i + 1)} \sum_{J^\pi} (2J + 1)\rho_{J^\pi}, \tag{9}$$

where $\rho_{J^\pi} = 1/D_{J^\pi}$ is the level density and $\langle \Gamma^{(r)} \rangle$ is given by Eq. (34). Note that the sum in Eq. (9) is the total density of states, which can be found without constructing states with definite J.
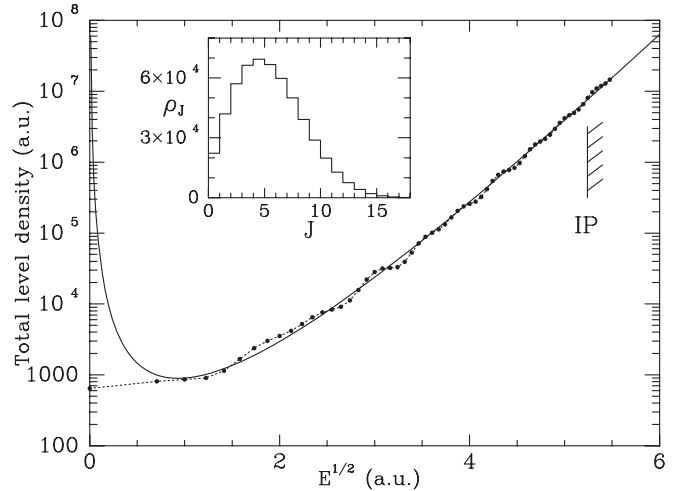

FIG. 2. Level density in Au^{24+}. The black dots are the result of the numerical calculation [7]. The solid line is the analytical fit, $\rho(E) = AE^{-\nu} \exp(a\sqrt{E})$, motivated by the level density calculated using the Fermi gas model [1,7]. The inset shows the densities of states with different J at ionization energy $E = I$.

To estimate the recombination cross section in the general case one can use the following formula:

$$\bar{\sigma}_r \approx \frac{\bar{\sigma}_c \bar{\sigma}_r^a}{\bar{\sigma}_c + \bar{\sigma}_r^a}. \tag{10}$$

It follows from Eqs. (7)–(9) if ω_f does not depend on J.

B. Nature of chaotic compound states

The density of excited states $\rho(E)$ in a many-electron ion, especially with an open shell, increases rapidly (exponentially) as the number of excited electrons increases. Consider n electrons that can be distributed among a number of single-electron states $g = \sum_l 2(2l + 1)$, where l is the orbital angular momentum of the subshells available. The total number of many-body states that can be constructed is given by

$$\frac{g!}{n!(g - n)!} \approx \frac{\exp[n \ln(g/n) + n]}{\sqrt{2\pi n}}, \tag{11}$$

where we used the Stirling formula and assumed $g \gg n$.

Equation (11) indicates exponential increase of the number of many-electron states and the corresponding decrease of the energy interval between them as the number of "active" electrons n increases. For example, Fig. 2 shows how the density of multielectron excited states of Au^{24+} increases with energy E. The small level spacings between the states mean that even a small residual electron-electron interaction will cause strong nonperturbative mixing of the many-electron configuration basis states (Slater determinants) $|\Phi_k\rangle$. This occurs when the off-diagonal matrix elements of the Hamiltonian H_{ij} become greater than the energy spacing D_{ij} between the basis states i and j coupled by the residual interaction, $H_{ij} > D_{ij}$.

When the mixing is strong, each eigenstate

$$|\Psi_\nu\rangle = \sum_k C_k^{(\nu)} |\Phi_k\rangle \tag{12}$$

contains a large number N of *principal components* $|\Phi_k\rangle$, i.e., basis states for which the expansion coefficients have typical
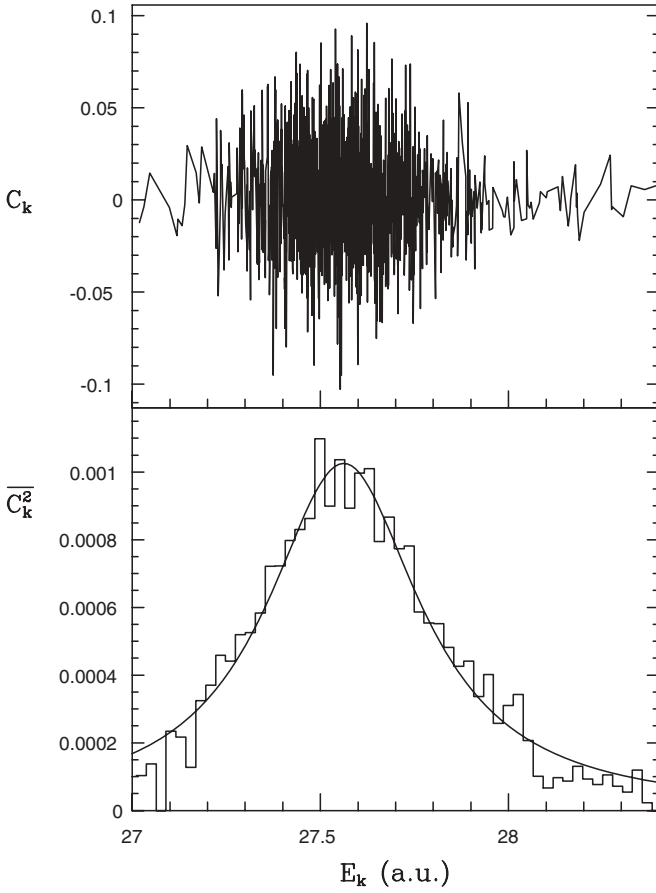
FIG. 3. Components of the 590th eigenstate with $J^{\pi} = 13/2^{-}$ in Au^{24+} from a two-configuration calculation [7] and $\overline{C_k^2}(E)$ (histogram) fit by the Breit-Wigner formula, Eq. (14) (solid line). The two configurations, $4f_{5/2}^3 4f_{7/2}^3 5p_{1/2}5p_{3/2}5f_{7/2}$ and $4f_{5/2}^3 4f_{7/2}^3 5p_{1/2}5d_{3/2}5g_{7/2}$, produce a total of 143 360 many-electron states with J from $\frac{1}{2}$ to $\frac{35}{2}$.

values $C_k^{(\nu)} \sim 1/\sqrt{N}$. (Recall the normalization condition $\sum_k |C_k^{(\nu)}|^2 = 1$.) The number of principal components can be estimated as $N \sim \Gamma_{spr}/D$, while the spreading width is given by the golden-rule-like formula

$$\Gamma_{spr} \simeq \frac{2\pi \overline{H_{ij}^2}}{D}, \tag{13}$$

and D is the mean level spacing between the basis states (or eigenstates). Such eigenstates are called compound states and are well known, e.g., in nuclear physics literature [1]. Owing to the strong mixing, the only good quantum numbers that can be used to classify the eigenstates are the exactly conserved total angular momentum and parity J^{π}, and the energy.

For example, in Au^{24+} the mean spacing between the excited states with a given angular momentum and parity, near the ionization threshold, is $D_{J^{\pi}} \sim 1$ meV and $\Gamma_{spr} \sim 10$ eV, so that $N \sim \Gamma_{spr}/D \sim 10^4$ [7]. Numerical calculations involving a relatively small number of configurations confirm that in this case the eigenstates are indeed chaotic superpositions of the basis states (see Fig. 3).

The energies E_k of the principal basis components lie within the spreading width of the eigenenergy E_{ν} of the

compound state, $|E_k - E_{\nu}| \lesssim \Gamma_{spr}$. The components outside the spreading width decrease quickly, so that they do not give much contribution to the normalization. It was tested in Refs. [6,7] that components of the chaotic eigenstates have the statistics of Gaussian random variables with zero mean (Fig. 3, top). On the other hand, the variation of their mean-squared value as a function of energy (Fig. 3, bottom) is described well by the Breit-Wigner profile,

$$\overline{|C_k^{(\nu)}|^2} = N^{-1} \frac{\Gamma_{spr}^2/4}{(E_k - E_{\nu})^2 + \Gamma_{spr}^2/4}, \tag{14}$$

with $N = \pi \Gamma_{spr}/2D$ fixed by normalization,

$$\sum_k |C_k^{(\nu)}|^2 \simeq \int \overline{|C_k^{(\nu)}|^2} dE_k/D = 1. \tag{}$$

Note that the degree of mixing in such chaotic, compound states is effectively complete, i.e., all basis states that can be mixed (within a certain energy range) are mixed together. These states cannot be described in terms of electronic configurations, as each eigenstate contains significant contributions of all nearby configurations. These properties of chaotic compound states enable one to calculate mean-squared matrix elements of different operators without complete diagonalization of large configuration-interaction Hamiltonian matrices.

C. Mean-squared matrix elements between compound states

Consider a two-body operator (e.g., the Coulomb interaction)

$$\hat{V} = \frac{1}{2} \sum_{abch} \langle ab|\hat{v}|hc\rangle a_a^{\dagger} a_b^{\dagger} a_h a_c.$$

A matrix element of $\hat{V}$ between two compound states, $|\Psi_{\nu}\rangle$ and $|\Psi_i\rangle$, is given by [see Eq. (12)]

$$\langle \Psi_{\nu}|\hat{V}|\Psi_i\rangle = \sum_{kk'} C_k^{(\nu)*} C_{k'}^{(i)} \langle \Phi_k|\hat{V}|\Phi_{k'}\rangle \tag{15}$$

or

$$\langle \Psi_{\nu}|\hat{V}|\Psi_i\rangle = \frac{1}{4} \sum_{abch} (\langle ab|\hat{v}|hc\rangle - \langle ba|\hat{v}|hc\rangle)$$
$$\times \langle \Psi_{\nu}|a_a^{\dagger} a_b^{\dagger} a_h a_c|\Psi_i\rangle, \tag{16}$$

where $\langle \Psi_{\nu}|a_a^{\dagger} a_b^{\dagger} a_h a_c|\Psi_i\rangle$ determines the contribution of the two-particle transition $ch \to ab$. Due to the assumption that the expansion coefficients for chaotic compound states are random and uncorrelated ($\overline{C_k^{(\nu)}} = \overline{C_k^{(\nu)*} C_{k'}^{(i)}} = 0$ for $\nu \neq i$), the value of the matrix element averaged over many compound states ν is zero:

$$\overline{\langle \Psi_{\nu}|\hat{V}|\Psi_i\rangle} = 0, \quad \overline{\langle \Psi_{\nu}|a_a^{\dagger} a_b^{\dagger} a_h a_c|\Psi_i\rangle} = 0. \tag{17}$$

To determine the autoionization width (Sec. II D) we need to calculate the *mean-squared* matrix element. It is derived using the statistical properties of the expansion coefficients,

$\overline{C_k^{(\nu)*}C_l^{(\nu)}} = \overline{|C_k^{(\nu)}|^2}\delta_{kl}$, so that

$$\overline{\langle\Psi_\nu|a_a^\dagger a_b^\dagger a_c a_h|\Psi_i\rangle\langle\Psi_i|a_{c'}^\dagger a_{h'}^\dagger a_{b'}a_{a'}|\Psi_\nu\rangle}$$
$$= \delta_{aa'}\delta_{bb'}\delta_{cc'}\delta_{hh'}\overline{|\langle\Psi_\nu|a_a^\dagger a_b^\dagger a_h a_c|\Psi_i\rangle|^2} + \dots, \quad (18)$$

where the dots correspond to three analogous terms with permutations of a and b, and c and h. Hence, the mean-squared matrix element is

$$\overline{|\langle\Psi_\nu|\hat{V}|\Psi_i\rangle|^2} = \frac{1}{4}\sum_{abch}|\langle ab|\hat{v}|hc\rangle - \langle ba|\hat{v}|hc\rangle|^2$$
$$\times \overline{|\langle\Psi_\nu|a_a^\dagger a_b^\dagger a_h a_c|\Psi_i\rangle|^2}. \quad (19)$$

Let us introduce the strength function

$$w(E_k; E_\nu, \Gamma_{\rm spr}, N) \equiv \overline{C_k^{(\nu)2}}, \quad (20)$$

which describes the spreading of the component k over the eigenstates ν ($C_k^{(\nu)}$ are assumed to be real). This function depends on the number of principal components N of the eigenstate [Eq. (12)], the spreading width $\Gamma_{\rm spr}$, and the difference $E_\nu - E_k$ between the energies of the compound state and component k. In the simplest model [1] $w(E_k; E_\nu, \Gamma_{\rm spr}, N)$ is a Breit-Wigner function [cf. Eq. (14)]. Using Eq. (15), we then obtain

$$\overline{|\langle\Psi_\nu|a_a^\dagger a_b^\dagger a_h a_c|\Psi_i\rangle|^2}$$
$$= \sum_{kk'}\sum_{ll'}\overline{C_k^{(\nu)}C_l^{(\nu)}C_{k'}^{(i)}C_{l'}^{(i)}}$$
$$\times \langle\Phi_k|a_a^\dagger a_b^\dagger a_h a_c|\Phi_{k'}\rangle\langle\Phi_{l'}|a_c^\dagger a_h^\dagger a_b a_a|\Phi_l\rangle$$
$$= \sum_{kk'}w_i(E_{k'})w_\nu(E_k)$$
$$\times \langle\Phi_{k'}|a_c^\dagger a_h^\dagger a_b a_a|\Phi_k\rangle\langle\Phi_k|a_a^\dagger a_b^\dagger a_h a_c|\Phi_{k'}\rangle. \quad (21)$$

To obtain the last expression we used the properties of the components and the definition (20), and denoted $w_i(E_{k'}) \equiv w(E_{k'}; E_i, \Gamma_{\rm spr}^{(i)}, N_i)$ and $w_\nu(E_k) \equiv w(E_k; E_\nu, \Gamma_{\rm spr}^{(\nu)}, N_\nu)$.

We can assume, without the loss of generality, that the number of principal components $|\Phi_k\rangle$ in state ν is greater than or equal to the number of components $|\Phi_{k'}\rangle$ of state i, i.e., $\Gamma_{\rm spr}^{(\nu)}/D_\nu \geqslant \Gamma_{\rm spr}^{(i)}/D_i$. The matrix element $\langle\Phi_k|a_a^\dagger a_b^\dagger a_h a_c|\Phi_{k'}\rangle$ does not vanish only if $|\Phi_k\rangle = a_a^\dagger a_b^\dagger a_h a_c|\Phi_{k'}\rangle$, so that $E_k - E_{k'} \simeq \varepsilon_a + \varepsilon_b - \varepsilon_h - \varepsilon \equiv \omega_{ab,ch}$. Using closure to sum over k in Eq. (21), we obtain

$$\overline{|\langle\Psi_\nu|a_a^\dagger a_b^\dagger a_h a_c|\Psi_i\rangle|^2} = \sum_{k'}w_i(E_{k'})w_\nu(E_{k'} + \omega_{ab,ch})$$
$$\times \langle\Phi_{k'}|\hat{n}_h\hat{n}_c(1-\hat{n}_a)(1-\hat{n}_b)|\Phi_{k'}\rangle. \quad (22)$$

In deriving this equation we used the anticommutation relations satisfied by the creation and annihilation operators, and introduced the occupation number operators $\hat{n}_a = a_a^\dagger a_a$. The matrix element $\langle\Phi_{k'}|\hat{n}_h\hat{n}_c(1-\hat{n}_a)(1-\hat{n}_b)|\Phi_{k'}\rangle$ is equal to unity if the orbitals h and c are occupied, while the orbitals a and b are vacant in the state $|\Phi_{k'}\rangle$, i.e., the transition $ch \rightarrow ab$ is possible.

If one assumes that the single-electron-state occupancies vary slowly with the excitation energy, then the matrix element of the operator $\hat{n}_h\hat{n}_c(1-\hat{n}_a)(1-\hat{n}_b)$ in Eq. (22) can be replaced by its expectation value,

$$\sum_{k'}w_i(E_{k'})\langle\Phi_{k'}|\hat{n}_h\hat{n}_c(1-\hat{n}_a)(1-\hat{n}_b)|\Phi_{k'}\rangle$$
$$= \langle\hat{n}_h\hat{n}_c(1-\hat{n}_a)(1-\hat{n}_b)\rangle_i, \quad (23)$$

subject to the normalization condition $\sum_{k'}w_i(E_{k'}) = 1$. The right-hand side of Eq. (23) is the value of the occupancy times "emptiness" in the compound state $|\Psi_i\rangle$, averaged over a number of neighboring states.

Replacing the matrix element $\langle\Phi_{k'}|\cdots|\Phi_{k'}\rangle$ by its average (23) in Eq. (22), and changing summation to integration, one obtains

$$\overline{|\langle\Psi_\nu|a_a^\dagger a_b^\dagger a_c a_h|\Psi_i\rangle|^2} = \langle\hat{n}_h\hat{n}_c(1-\hat{n}_a)(1-\hat{n}_b)\rangle_i$$
$$\times \int w_i(E_{k'})w_\nu(E_{k'} + \omega_{ab,ch})\frac{dE_{k'}}{D_i}. \quad (24)$$

This result can be written in the following form:

$$\overline{|\langle\Psi_\nu|a_a^\dagger a_b^\dagger a_h a_c|\Psi_i\rangle|^2} = \langle\hat{n}_h\hat{n}_c(1-\hat{n}_a)(1-\hat{n}_b)\rangle_i$$
$$\times D_\nu\tilde{\delta}(\Gamma_{\rm spr}^{(i)}, \Gamma_{\rm spr}^{(\nu)}, \Delta). \quad (25)$$

In this expression,

$$\tilde{\delta}(\Gamma_{\rm spr}^{(i)}, \Gamma_{\rm spr}^{(\nu)}, \Delta) \equiv \frac{1}{D_\nu}\int w(E_{k'}; E_i, \Gamma_{\rm spr}^{(i)}, N_i)$$
$$\times w(E_{k'} + \omega_{ab,ch}; E_\nu, \Gamma_{\rm spr}^{(\nu)}, N_\nu)\frac{dE_{k'}}{D_i}, \quad (26)$$

where $\Delta \equiv E_\nu - E_i - \omega_{ab,ch}$ is a "spread" δ function, which was studied in Refs. [2,3,6]. It peaks at $\Delta = 0$ and describes the approximate energy conservation for the transition between compound states induced by the two-electron transition $ch \rightarrow ab$ and broadened by the spreading widths. For the Breit-Wigner strength functions one has

$$\tilde{\delta}(\Gamma_{\rm spr}^{(i)}, \Gamma_{\rm spr}^{(\nu)}, \Delta) = \frac{1}{2\pi}\frac{\Gamma_{\rm spr}}{\Delta^2 + \Gamma_{\rm spr}^2/4}, \quad (27)$$

where $\Gamma_{\rm spr} = \Gamma_{\rm spr}^{(i)} + \Gamma_{\rm spr}^{(\nu)}$. From Eqs. (19) and (25), the mean-squared matrix element of the two-body operator between the compound states is finally obtained as

$$\overline{|\langle\Psi_\nu|\hat{V}|\Psi_i\rangle|^2} = \frac{1}{4}\sum_{abch}|\langle ab|\hat{v}|hc\rangle - \langle ba|\hat{v}|hc\rangle|^2$$
$$\times \langle\hat{n}_h\hat{n}_c(1-\hat{n}_a)(1-\hat{n}_b)\rangle_i D_\nu\tilde{\delta}(\Gamma_{\rm spr}^{(i)}, \Gamma_{\rm spr}^{(\nu)}, \Delta). \quad (28)$$

In this expression the summation is carried out over the single-electron states a, b, h, and c. Note that if $|\Psi_i\rangle$ is a simple, unmixed state, there is no sum over k' in Eqs. (21)–(23). In this case $\Gamma_{\rm spr}^{(i)} = 0$ and $\Gamma_{\rm spr} = \Gamma_{\rm spr}^{(\nu)}$ in Eq. (27).

For a one-body operator $\hat{M} = \sum_{ab} M_{ab} a_a^\dagger a_b$, the mean-squared matrix element is obtained similarly [2,3,6]:

$$\overline{|\langle \Psi_\nu | \hat{M} | \Psi_f \rangle|^2} = \sum_{ab} |\langle a | \hat{m} | b \rangle|^2 \langle \hat{n}_a (1 - \hat{n}_b) \rangle_\nu$$
$$\times D_f \tilde{\delta}\left(\Gamma_{\rm spr}^{(\nu)}, \Gamma_{\rm spr}^{(f)}, E_f - E_\nu - \omega_{ba}\right), \quad (29)$$

where $\omega_{ba} = \varepsilon_b - \varepsilon_a$ is the energy of the single-electron transition $a \to b$.

D. Capture cross section and autoionization width

The autoionization width $\Gamma_\nu^{(a)} = 2\pi |\langle \Psi_\nu | \hat{V} | \Psi_i \rangle|^2$ gives the transition rate between the initial state, $e^- + A^{q+}$, and the multiply exited compound resonance of the ion $A^{(q-1)+}$ due to the two-body Coulomb interaction $\hat{V}$. Unlike the complex multiply excited states $|\Psi_\nu\rangle$, the initial state of the recombination process is simple. It describes an electron with the energy ε incident on the ground (or low-lying excited) state $|\Phi_0\rangle$ of the target, which is often dominated by one configuration. It is clear that the autoionization width averaged over compound resonances is determined by the mean-squared matrix element of the Coulomb interaction between electrons, which is given by Eq. (28). The initial state $|\Psi_i\rangle = |\Phi_0, c\rangle$ is thus a compound state with negligible spreading width $\Gamma_{\rm spr}^{(i)} \ll \Gamma_{\rm spr}^{(\nu)}$. The total width of the function $\tilde{\delta}$ [Eq. (27)] is dominated by the compound resonance width $\Gamma_{\rm spr} \approx \Gamma_{\rm spr}^{(\nu)}$.

Nonzero contributions to the sum in Eq. (28), i.e., to $\Gamma^{(a)}$, arise from the basis states, which differ from the initial state $|\Phi_0, c\rangle$ by the single-particle states of two electrons. Therefore, it is sufficient to sum over the doubly excited basis states,

$$\Gamma^{(a)} = 2\pi \sum_d \overline{C_d^{(\nu)2}} |\langle \Phi_d | \hat{V} | \Phi_0, c \rangle|^2.$$

Such two-electron excitations $|\Phi_d\rangle$ play the role of *doorway states* for the electron capture process. Since these states are not the eigenstates of the system, they have a finite energy width $\Gamma_{\rm spr}$. The wave function of a doorway state can be constructed using the creation-annihilation operators $|\Phi_d\rangle = a_a^\dagger a_b^\dagger a_h |\Phi_0, c\rangle$, where $a \equiv n_a l_a j_a m_a$ and $b \equiv n_b l_b j_b m_b$ are excited single-electron states, and $h \equiv n_h l_h j_h m_h$ corresponds to the hole in the target ground state. Of course, to form the doorway states with a given total angular momentum J, the excited electrons and the ionic residue must be coupled into J. However, the $2J + 1$ factor and summation over J in Eq. (8) account for all possible couplings. This means that the sum over the eigenstates in Eq. (8) can be replaced by the sum over the one-hole–two-electron excitation, as in Eq. (28), and one obtains the capture cross section in the form of Eq. (1).

Note that when the number of active electrons and orbitals is large, the occupation numbers for different orbitals become statistically independent. In this case, the correlated product of the single-particle occupancies, Eq. (23), can be approximated by the fractional occupation numbers of the electronic *subshells* with definite j. The orbital c is taken as a continuum, $c \equiv \varepsilon l j m$, in Eq. (1). Its wave function is normalized to the δ function of energy, and it is occupied in the initial state, i.e., $\hat{n}_c = 1$. After summation over the magnetic quantum numbers m_a, m_b, etc. and angular reduction of the Coulomb matrix

elements, the final expression for the capture cross section is

$$\bar{\sigma}_c = \frac{\pi^2}{k^2} \sum_{abh,lj} \frac{\Gamma_{\rm spr}}{(\varepsilon - \varepsilon_a - \varepsilon_b + \varepsilon_h)^2 + \Gamma_{\rm spr}^2/4}$$
$$\times \sum_\lambda \frac{\langle a, b \| V_\lambda \| h, \varepsilon l j \rangle}{2\lambda + 1} \left[\langle a, b \| V_\lambda \| h, \varepsilon l j \rangle - (2\lambda + 1) \right.$$
$$\times \sum_{\lambda'} (-1)^{\lambda + \lambda' + 1} \left\{ \begin{array}{ccc} \lambda & j_a & j \\ \lambda' & j_b & j_h \end{array} \right\} \langle b, a \| V_{\lambda'} \| h, \varepsilon l j \rangle \right]$$
$$\times \frac{n_h}{2j_h + 1} \left(1 - \frac{n_a}{2j_a + 1}\right)\left(1 - \frac{n_b}{2j_b + 1}\right). \quad (30)$$

Here n_a, n_b, and n_h are the occupation numbers of the corresponding subshells (ranging from 0 to $2j_a + 1$, etc.), and ε_a, ε_b, and ε_h are their energies. The two terms in square brackets represent the direct and exchange contributions, and $\langle a, b \| V_\lambda \| h, \varepsilon l j \rangle$ is the reduced Coulomb matrix element,

$$\langle a, b \| V_\lambda \| h, c \rangle = \sqrt{(2j_a + 1)(2j_b + 1)(2j_h + 1)(2j_c + 1)}$$
$$\times \xi(l_a + l_c + \lambda)\xi(l_b + l_h + \lambda)$$
$$\times \begin{pmatrix} \lambda & j_a & j_c \\ 0 & -\frac{1}{2} & \frac{1}{2} \end{pmatrix} \begin{pmatrix} \lambda & j_b & j_h \\ 0 & -\frac{1}{2} & \frac{1}{2} \end{pmatrix} R_\lambda(a, b; h, c),$$
$$(31)$$

where $\xi(L) = [1 + (-1)^L]/2$ is the parity factor and

$$R_\lambda(a, b; h, c) = \iint \frac{r_<^\lambda}{r_>^{\lambda+1}} [f_a(r) f_c(r) + g_a(r) g_c(r)]$$
$$\times [f_b(r') f_h(r') + g_b(r') g_h(r')] dr dr' \quad (32)$$

is the radial Coulomb integral, f and g being the upper and lower components of the relativistic orbital spinors.

Once $\bar{\sigma}_c$ is known, Eq. (8) allows one to estimate the average ratio $\Gamma^{(a)}/D$ for a typical J^π,

$$\left\langle \frac{\Gamma^{(a)}}{D} \right\rangle = \frac{k^2 (2J_i + 1) \bar{\sigma}_c}{\pi^2 \sum_{J^\pi} (2J + 1)} = \frac{k^2 (2J_i + 1) \bar{\sigma}_c}{2\pi^2 J_{\max}^2}, \quad (33)$$

where the sum in the denominator is over the angular momentum and parity J^π, which contribute effectively to the capture cross section. For example, $J_{\max} \approx 10$ and $J_i = 6$ for the recombination of Au^{25+} and W^{20+}. A typical distribution of level densities ρ_{J^π} for different J is shown on the inset of Fig. 2.

E. Radiative width

The second step of the recombination process is radiative stabilization. Any excited electron in the compound state $|\Psi_\nu\rangle$ can emit a photon. Using Eq. (29), the total photoemission rate $\Gamma^{(r)}$ can be estimated as a weighted sum of the single-particle rates,

$$\Gamma^{(r)} \simeq \sum_{a,b} \frac{4\omega_{ba}^3}{3c^3} |\langle a \| \hat{d} \| b \rangle|^2 \left\langle \frac{n_b}{2j_b + 1} \left(1 - \frac{n_a}{2j_a + 1}\right) \right\rangle_\nu,$$
$$(34)$$

where $\omega_{ba} = \varepsilon_b - \varepsilon_a > 0$, $\langle a \| \hat{d} \| b \rangle$ is the reduced dipole operator between the orbitals a and b, and $\langle \ldots \rangle_\nu$ is the mean occupation number factor. The mean subshell occupation

numbers for a given energy can be obtained by averaging over the basis states involved, e.g.,

$$n_a(E) = \sum_k \overline{C_k^2}(E) n_a^{(k)}, \qquad (35)$$

where $n_a^{(k)}$ is the occupation number of the subshell a in the basis state k.

Since $|\Psi_\nu\rangle$ have large numbers of principal components N, the fluctuations of their radiative widths are small, $\sim 1/\sqrt{N}$. This can also be seen if one recalls that a chaotic multiply excited state is coupled by photoemission to many lower-lying states, and the total radiative width is the sum of a large number of (strongly fluctuating) partial widths. A similar effect is known in compound nucleus resonances in low-energy neutron scattering [1,16]. In multicharged ions with dense spectra of chaotic multiply excited states, the autoionization widths are suppressed as $\Gamma^{(a)} \propto 1/N$. Physically this happens because the coupling strength of the two-electron doorways state to the continuum is shared between many complex, multiply excited eigenstates. The radiative width does not have this suppression, since all components of a compound state contribute to the radiative decay. As a result, the radiative width may dominate in the total width of the resonances, $\Gamma^{(r)} \gg \Gamma^{(a)}$, making their fluorescence yield close to unity. Our numerical results for the recombination of Au^{25+} presented in [8] support this picture.

III. NUMERICAL RESULTS

In this section we apply our theory to calculate the recombination rate for the tungsten ions from W^{17+} to W^{24+}. Experimental data are available for the recombination of W^{20+} forming W^{19+} [13]. We will use this system as an example to describe the calculations. Calculations for other ions are similar.

When an electron recombines with W^{20+}, it can be captured into an excited state of the compound W^{19+} ion. Its ground state belongs to the $1s^2 \ldots 4f^9$ configuration. Figure 4 shows the energies of its relativistic orbitals nlj obtained in the Dirac-Fock calculation. All orbitals below the Fermi level, $1s$ to $4f$, were obtained in the self-consistent calculation of the W^{19+}

FIG. 4. Energies of the occupied and vacant single-particle orbitals of W^{19+} obtained in the Dirac-Fock calculation.

ground state. Each of the excited-state orbitals above the Fermi level: $5s$, $5p$, etc., was calculated by placing one electron into it, in the field of the frozen $W^{20+} 1s^2 \ldots 4f^8$ core. The energy of the highest orbital occupied (partially) in the ground state is $\varepsilon_{4f_{7/2}} = -18.41$ a.u. This value gives an estimate of the ionization potential of W^{19+}: $I \approx |\varepsilon_{4f_{7/2}}| = 18.41$ a.u. This value is in agreement with NIST data, $I = 18.47$ a.u. [18].

Excited states of the ion are generated by transferring one, two, three, etc. electrons from the ground-state orbitals into the empty orbitals above the Fermi level (Fig. 4), or into the partially occupied $4f$ orbitals. We are interested in the excitation spectrum of W^{19+} near its ionization threshold. This energy ($\sim$20 a.u.) is sufficient to push up a few of the nine $4f$ electrons, and even excite one or two electrons from the $4d$ orbital. However, the preceding $4p$ orbital is already deep enough to be considered inactive. Thus, we treat W^{19+} as a system of 19 electrons above the frozen Kr-like $1s^2 \ldots 4p^6$ core. Note that in constructing the excited-state configurations, we disregard infinite Rydberg series which correspond to the excitation of one electron in the field of W^{20+}. Rydberg states belong to a single-particle aspect of the $e^- + W^{20+}$ problem and are not expected to contribute much to the recombination cross section in this system.

Assuming that the fluorescence yield is close to unity (see below), we calculate the recombination cross section from Eq. (30). Before using this formula, one needs to obtain a list of two-electron–one-hole excitations of W^{19+} with energies close to the ionization threshold, which act as the doorway states. One also needs to estimate the spreading width Γ_{spr}. For low-energy electron recombination, we restrict the consideration to the energy interval,

$$E = I \pm \Delta E / 2, \qquad (36)$$

where the energy is measured from the ground state of the final-state ion, and we choose $\Delta E \sim \Gamma_{spr}$. In practice, we start from some initial estimate of the spreading width and subsequently find a more accurate value using an iterative procedure.

The spreading width is obtained from Eq. (13), where the mean-squared off-diagonal Hamiltonian matrix element $\overline{H_{ij}^2}$ is found by averaging over N_s basis states whose energies $E_k \equiv H_{kk}$ lie within the energy interval (36), and $D = \Delta E / N_s$. The list of two-electron–one-hole excitations $h^{-1}ab$ which contribute to the sum (30) includes configurations with basis states in the interval (36). It is known that the spreading width is a robust characteristic of the system. Indeed, we have checked that when more configurations are included, both D and $\overline{H_{ij}^2}$ decrease, whereas Γ_{spr} does not change much (see also Ref. [9]).

When finding $\overline{H_{ij}^2}$ and D we use basis states with definite projection of the total angular momentum J_z corresponding to the minimal value of J_z (0 or 1/2), rather than the states with definite total angular momentum J. This method is significantly simpler than the use of the basis states with definite J and J_z, and produces the same results for Γ_{spr} [Eq. (13)].

Table I shows the spreading widths for the compound ions of tungsten $W^{(q-1)+}$, with excitation energies close to the ionization threshold, formed in the process of low-energy electron recombination with $W^{(q)+}$. With the exception of the target ion with the smallest number of $4f$ electrons
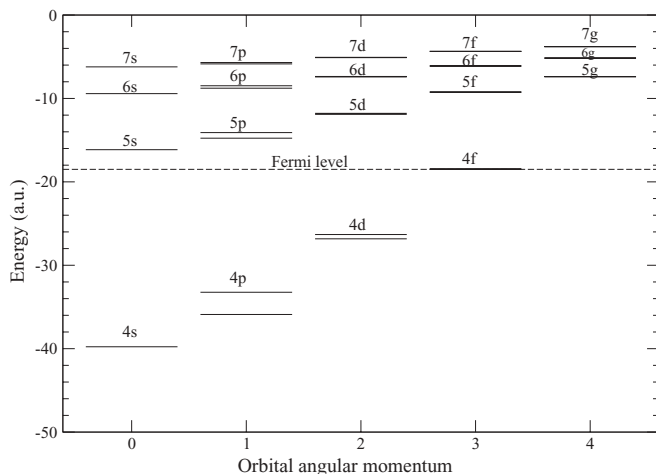
TABLE I. Electron capture cross sections $\bar{\sigma}_c$ and rate coefficients α_c for the tungsten ions $W^{(q)+}$ with the open $4f$ subshell, and properties of the compound ions $W^{(q-1)+}$ at excitation energies close to the ionization threshold I.

Target ion	I^a (a.u.)	D (10^{-4} a.u.)	K	Γ_{spr} (a.u.)	$\bar{\sigma}_c{}^b$ (10^{-16} cm^2)	$\alpha_c{}^b$ (10^{-7} cm^3/s)
$W^{18+}4f^{10}$	15.5	0.2	70	0.56	25	1.5
$W^{19+}4f^{9}$	17.0	0.1	93	0.65	29	1.7
$W^{20+}4f^{8}$	18.5	0.1	105	0.68	30	1.8
$W^{21+}4f^{7}$	20.0	0.1	96	0.68	34	2.0
$W^{22+}4f^{6}$	21.8	0.2	76	0.65	16	0.98
$W^{23+}4f^{5}$	23.5	0.4	48	0.59	11	0.67
$W^{24+}4f^{4}$	25.2	1.3	25	0.50	19	1.1
$W^{25+}4f^{3}$	27.0	11	5	0.16	12	0.7

[a]Ionization energy of the final-state ions (Ref. [18]).
[b]Capture cross section from Eq. (30) and rate coefficient for incident electron energy $\varepsilon = 1$ eV.

($W^{25+}4f^3$), the spreading widths are in the range 0.5–0.7 a.u. In fact, the value of Γ_{spr} does not strongly affect the magnitude of the capture cross section [Eq. (30)], since the area under the Breit-Wigner contour corresponding to each doorway $h^{-1}ab$ is independent of Γ_{spr}.

As discussed in Sec. II B, strong mixing of the basis states results in the eigenstates with large numbers of principal components, $N \sim \Gamma_{\mathrm{spr}}/D \sim \overline{H_{ij}^2}/D^2 \gg 1$. This occurs when

$$K = \sqrt{\overline{H_{ij}^2}}/D \gg 1. \tag{37}$$

Table I shows that this criterion is fulfilled for all the ions studied and that the expected number of principal components is indeed large, $N \sim 10^4$. As explained in Sec. II E, in this case one can expect large fluorescence yields, $\omega_f \approx 1$. This means that the recombination cross section will be at the limit given by the total electron capture cross section [Eq. (30)].

In the present calculations of $\bar{\sigma}_c$ [Eq. (30)], we also include in a semiempirical way the effect of screening of the Coulomb interaction between valence electrons by core electrons. This is done by introducing the screening factors f_λ in the two-electron Coulomb integrals, assuming that these factors depend on the Coulomb integral multipolarity λ only. The factors were calculated to be $f_1 = 0.7$, $f_2 = 0.8$, $f_3 = 0.9$ [19]. Coulomb integrals of other multipolarities are not modified. The above values of the screening factors were found in the calculations for other atomic systems. However, in practice they change little from one atom to another.

To compare with experiment for W^{20+} [13], the cross section obtained from Eq. (30) is converted into the rate coefficient $\alpha_c = \bar{\sigma}_c v$, where v is the velocity of the incident electron. The result is shown in Fig. 5 by the solid line. Since the sum in Eq. (30) has a weak dependence on the electron energy, the capture cross section at low energies is proportional to $1/\varepsilon$, and the corresponding rate coefficient behaves as $\alpha_c \propto 1/v$. The calculated rate agrees well with the experimental data in the energy range of 0.1–1 eV. At higher energies the experimental rate coefficient tends to drop faster than $1/v$.
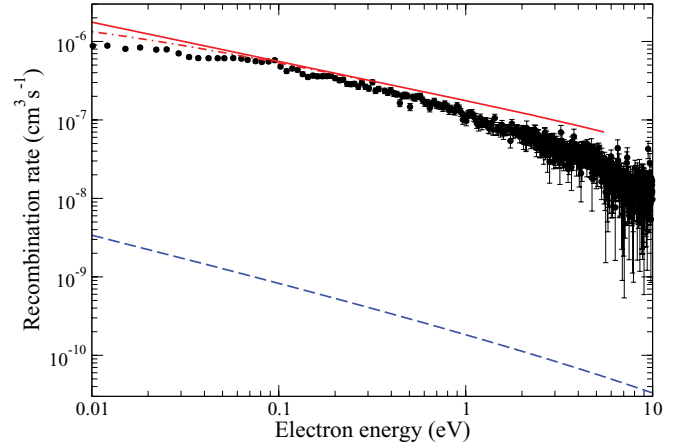

FIG. 5. (Color online) Recombination rate coefficient of W^{20+}. Dashed line is the direct radiative recombination rate, Eq. (38); solid line is the capture rate calculated using the present theory, Eq. (30); dot-dashed line shows the same, taking into account the velocity distribution of the electron beam (see text); solid circles represent the measured rate coefficient [13].

Figure 5 also shows the rate coefficient for the direct radiative recombination. The latter is estimated using the Kramers formula for the radiative recombination cross section [20] (in atomic units),

$$\sigma_d^r = \frac{32\pi}{3\sqrt{3}c^3} \frac{Z_i^2}{k^2} \ln\left(\frac{Z_i}{n_0 k}\right), \tag{38}$$

where Z_i is the ionic charge (e.g., $Z_i = 20$ for $e^- + W^{20+}$), and n_0 is the principal quantum number of the lowest unoccupied ionic orbital ($n_0 = 5$ for W^{20+}) [7]. The energy dependence of this cross section is close to $1/\varepsilon$, and the corresponding rate coefficient (dashed line in Fig. 5) is 3 orders of magnitude smaller than the measurement in the energy range shown.

Below $\varepsilon = 0.1$ eV the measured recombination rate coefficient can be affected by the velocity distribution of the electron beam, which is characterized by two temperatures, $T_\parallel = 0.15$ meV and $T_\perp = 10$ meV [13]. Taking this into account (see Eq. (18) in Ref. [8]) reduces the calculated resonant capture rate below 50 meV (dot-dashed line in Fig. 5), bringing it into closer agreement with experiment. At higher energies, inelastic (electronic excitation) channels open, and the fluorescence yield can drop below unity, reducing the recombination rate relative to that of resonant capture. Also, the ground-state configuration of $W^{20+}4d^{10}4f^8$ contains 293 closely spaced fine-structure levels [13]. A few of these are long lived and can be present in the ion beam, which may contribute to reduced values of the fluorescence yield.

As discussed above, the capture cross section has a simple $1/\varepsilon$ energy dependence at low electron energies. Hence, in Table I we show the cross sections and rate coefficients for W^{q+} ($q = 18$–25) calculated at one low electron energy, $\varepsilon = 1$ eV. We see that the largest cross section is predicted for the ion with the half-filled $4f$ subshell. On the other hand, all the cross sections are within a factor of 3 of each other, and much larger than what one would expect from the direct RR process [Eq. (38)].

Of course, one must keep in mind that compared with the capture cross section, the recombination cross section

contains an additional factor ω_f. The fluorescence yield may be significantly smaller than $\omega_f = 1$ for ions, in which the degree of mixing is not as large as it is in the compound W^{19+} ion. In particular, this may be the case for the ions in which the mixing strength K (see Table I) and the number of principle components N is not too large. In this case one should regard $\bar{\sigma}_c$ as the upper limit, and use Eqs. (9) and (10) to estimate the recombination cross section.

IV. CONCLUSIONS

A detailed derivation of the statistical theory of resonant electron capture by many-electron ions has been presented. Numerical calculations have been performed for a number of tungsten ions with a partially filled $4f$ subshell. The calculated rate coefficient for W^{20+} is in agreement with the measurements at low electron energy. The present approach can be used to investigate other processes mediated by chaotic, multielectronic excited states.

Note added: Recently we became aware of the work by Badnell *et al.* [21]. Their extensive calculation of dielectronic recombination of W^{20+} underestimates the experimental recombination rate at low energies by a factor of 3, but it achieves agreement with experiment by "partitioning" the autoionization rates using the Breit-Wigner distribution with a spreading width of 10 eV.

[1] A. Bohr and B. Mottelson, *Nuclear Structure* (Benjamin, New York, 1969), Vol. 1.

[2] V. V. Flambaum, Phys. Scr. T **46**, 198 (1993); V. V. Flambaum and O. K. Vorov, Phys. Rev. Lett. **70**, 4051 (1993).

[3] V. V. Flambaum and G. F. Gribakin, Prog. Part. Nucl. Phys. **35**, 423 (1995).

[4] V. Zelevinsky, B. A. Brown, M. Frazier, and M. Horoi, Phys. Rep. **276**, 85 (1996).

[5] V. V. Flambaum and G. F. Gribakin, Philos. Mag. B **80**, 2143 (2000).

[6] V. V. Flambaum, A. A. Gribakina, G. F. Gribakin, and M. G. Kozlov, Phys. Rev. A **50**, 267 (1994); V. V. Flambaum, A. A. Gribakina, and G. F. Gribakin, *ibid.* **54**, 2066 (1996); **58**, 230 (1998); A. A. Gribakina, V. V. Flambaum, and G. F. Gribakin, Phys. Rev. E **52**, 5667 (1995); V. V. Flambaum, A. A. Gribakina, G. F. Gribakin, and I. V. Ponomarev, *ibid.* **57**, 4933 (1998); Physica D **131**, 205 (1999).

[7] G. F. Gribakin, A. A. Gribakina, and V. V. Flambaum, Aust. J. Phys. **52**, 443 (1999); arXiv:physics/9811010.

[8] V. V. Flambaum, A. A. Gribakina, G. F. Gribakin, and C. Harabati, Phys. Rev. A **66**, 012713 (2002).

[9] G. F. Gribakin and S. Sahoo, J. Phys. B **36**, 3349 (2003).

[10] M. Tokman, N. Eklow, P. Glans, E. Lindroth, R. Schuch, G. Gwinner, D. Schwalm, A. Wolf, A. Hoffknecht, A. Müller, and S. Schippers, Phys. Rev. A **66**, 012703 (2002); M. Schnell, G. Gwinner, N. R. Badnell, M. E. Bannister, S. Böhm, J. Colgan, S. Kieslich, S. D. Loch, D. Mitnik, A. Müller, M. S. Pindzola, S. Schippers, D. Schwalm, W. Shi, A. Wolf, and S.-G. Zhou, Phys. Rev. Lett. **91**, 043001 (2003).

[11] A. Hoffknecht, O. Uwira, S. Schennach, A. Frank, J. Haselbauer, W. Spies, N. Angert, P. H. Mokler, R. Becker, M. Kleinod, S. Schippers, and A. Müller, J. Phys. B **31**, 2415 (1998).

[12] O. Uwira, A. Müller, W. Spies, J. Linkemann, A. Frank, T. Cramer, L. Empacher, R. Becker, M. Kleinod, P. H. Mokler, J. Kenntner, A. Wolf, U. Schramm, T. Schiissler, D. Schwalm, and D. Habs, Hyperfine Interact. **99**, 295 (1996).

[13] S. Schippers, D. Bernhardt, A. Müller, C. Krantz, M. Grieser, R. Repnow, A. Wolf, M. Lestinsky, M. Hahn, O. Novotný, and D. W. Savin, Phys. Rev. A **83**, 012711 (2011).

[14] M. Lestinsky, N. R. Badnell, D. Bernhardt, M. Grieser, J. Hoffmann, D. Lukić, A. Müller, D. A. Orlov, R. Repnow, D. W. Savin, E. W. Schmidt, M. Schnell, S. Schippers, A. Wolf, and D. Yu, Astrophys. J. **698**, 648 (2009).

[15] N. Bohr, Nature (London) **137**, 344 (1936).

[16] V. V. Flambaum and O. P. Sushkov, Nucl. Phys. A **412**, 13 (1984); **435**, 352 (1985).

[17] L. D. Landau and E. M. Lifshitz, *Quantum Mechanics*, 3rd ed. (Pergamon, Oxford, 1977).

[18] Yu. Ralchenko, A. E. Kramida, J. Reader, and NIST ASD Team (2011). NIST Atomic Spectra Database (ver. 4.1.0), [Online]. Available: http://physics.nist.gov/asd [2012, February 21]. National Institute of Standards and Technology, Gaithersburg, MD.

[19] V. A. Dzuba, Phys. Rev. A **78**, 042502 (2008).

[20] I. I. Sobelman, *Atomic Spectra and Radiative Transitions* (Springer, Berlin, 1992).

[21] N. R. Badnell, C. P. Ballance, D. C. Griffin, and M. O'Mullane, Phys. Rev. A **85**, 052716 (2012).